

Influence of numerical methods on the simulation of the steady and unsteady two-phase flow in solid rocket motors

Valentin DUPIF^{*,♦,†}, Marc MASSOT^{♦,*,▼}, Joël DUPAYS^{*}, Frédérique LAURENT^{♦,▼} and Clément LE TOUZE^{*}

^{*}Fundamental and applied Energetics Department, ONERA 91123 Palaiseau FRANCE

valentin.dupif@onera.fr; joel.dupays@onera.fr; clement.le_touze@onera.fr

[♦]EM2C-CNRS, UPR 288 - "Laboratoire d'Énergétique Moléculaire et Macroscopique, Combustion"

CentraleSupélec, Grande Voie des Vignes 92295 Châtenay-Malabry FRANCE

marc.massot@centralesupelec.fr; frederique.laurent@centralesupelec.fr

[▼] FM, Fédération de Mathématiques de l'Ecole Centrale Paris, FR CNRS 3487

...
†Corresponding author

Abstract

The addition of aluminum powder in the propellant of Solid Rocket Motors improves performance but leads to a massive amount of aluminum oxide droplets in the combustion chamber. Complex coupling can occur in the chamber between gaseous hydrodynamic instabilities, acoustics and the moderately dense condensed liquid phase flow and lead to thrust oscillations. Droplet size, as confirmed by experiments, can have a strong impact on the onset/damping of oscillations. Numerical simulations of such complex physics face a challenge at three levels: 1- proper modeling of the disperse liquid phase, 2- efficient and accurate numerical methods for the resolution of the coupled problem, 3- high performance computing. Fully Eulerian models are investigated since they lead to efficient coupling and ease of parallelism through domain decomposition. However, they are also subject to singularity development and require specific numerical methods with a proper balance between accuracy and robustness. We investigate the influence of the choice of numerical schemes and mesh refinement on the ability to properly capture complex coupling of the phases and predict unstable behaviors. Two test-cases are chosen, typical of solid propulsion. Some recent effort in terms of numerical schemes in the CEDRE code at ONERA is shown to provide a reliable solution, even if great care has to be taken in order to get converged solutions.

1. Introduction

Rocket engines using solid propellant are commonly used for the first stages of space launchers. Aluminum powder is generally introduced in the propellant in a significant proportion to increase the flame temperature and the motor performances. But the expected gain is lowered by the presence of a massive amount, often up to more than 30% by weight, of aluminum oxide (Al_2O_3) residues and smokes in the combustion products. This condensed phase tends to reduce the ejection gas velocity through a drag effect in the expanding nozzle. The resulting so-called "two-phase losses" are generally the main contribution of the total performance loss that affects nozzle efficiency.^{1,2} Besides, large solid rocket motors (SRM) often exhibit, during firing, pressure oscillations essentially locked on first longitudinal acoustic modes. These longitudinal instabilities cause thrust oscillations which may lead to deleterious effect on motor ballistics and may affect launcher systems, components and payloads. The oscillations may result from very complex interactions between acoustic waves, that propagate in the confined volume of the chamber, and various transient or unsteady processes. Among those are, for instance, the unsteady propellant combustion,^{3,4} flow instabilities either developing downstream some discontinuities of the internal geometry^{5,6} or generated by a pure, intrinsic hydrodynamic instability of the flow injected from a lateral wall,^{7,8} the distributed combustion of aluminum droplets,^{9,10} or a combination of several of these factors.¹¹ The impact of the condensed phase on nozzle efficiency is clearly negative while it is generally more complex and ambiguous on pressure oscillations, especially when vortex shedding driven oscillations is developing. Both damping and driving mechanisms may be observed depending on various factors.¹²

Because of the aggressive and enclosed environment in which the flow occurs, experimental measurement possibilities are limited and numerical simulations are mandatory. Such numerical simulations need to be predictive and reproduce the complex interactions occurring between the gas and the particles with strong two-way coupling in order to both understand and analyze the physics involved as well as to provide reliable performance and stability predictions for applications. Whereas the description of the carrier gaseous flow field relies on Navier-Stokes conservation equations, several levels of description of the disperse condensed particle/droplet phase can be adopted. Thanks to their abilities to treat efficiently the exchange of conservative quantities between the carrier gas and the carried disperse particles, models based on fully Eulerian frameworks are well-suited candidates to tackle this issue. At least as a complementary modeling approach compared to Discrete Particle Simulations or Lagrangian stochastic particle discretization, a Eulerian description of the disperse phase offers several advantages beyond the coupling efficiency : no convergence issues as well as a lower cost, especially in the framework of unsteady and coalescing spray flows.¹³ Furthermore, the resulting fully Eulerian model allows an efficient parallelization through domain decomposition and are therefore highly interesting for industrial simulations and high performance computation.

Together with the particle mass loading, the particle size is a key parameter to reproduce correctly the impact of the condensed phase on the internal flow. Such issues have driven the development of the ONERA CEDRE code for several years. For SRMs issues, the modeling must be able to describe the initial particle size distribution and its subsequent evolutions throughout the chamber and the nozzle resulting from interactions with the flow as well as particle-particle interactions. A long-term effort has been conducted in the vicinity of the authors in order to develop Eulerian models, which can describe properly spray polydispersity and related dynamics, evaporation, heating, as well as break-up and coalescence. Models using size discretization from low order to high order moment methods and hybrid methods (see¹⁴⁻¹⁷ and references therein) have been successfully integrated for industrial configurations.^{13, 18, 19} In the framework of SRMs, the flexibility and accuracy of a hybrid two-size moment method coupled to a size phase space discretization within a few size intervals called sections (see¹⁷ and references therein for a broader view on the literature in this field) has proven to be an efficient solution. The field of treating polydispersity in size can be considered to have reached a mature level.

Eulerian models of sprays with finite inertia offer another difficulty related to the chosen closure using moment in velocity, potentially conditioned by droplet size. Depending on the size of the particles/droplets, and more specifically on their inertia described through a Stokes number, several models and closures can be envisioned depending on the occurrence of Particle Trajectory Crossing (PTC - deterministic or statistical in turbulent flows). Whereas the original monokinetic closure has been clarified theoretically in,^{14, 15} several possibility can be envisioned in order to treat crossing and we refer to^{20, 21} and references therein. The main difficulty resulting from such modeling is the intrinsic occurrence of singularities in the equations, which, even if the mathematical framework has been identified,^{21, 22} requires specific numerical methods in order to reach robustness, while preserving a high level of accuracy, especially in the framework of unstructured meshes. The monokinetic model has been implemented in the in-house SIERRA code, for structured SRM simple geometries, and in CEDRE for complex geometries and industrial configurations; it has shown to provide reliable results in several configurations involving low inertia particles. Since its weakly hyperbolic character leads to identified strong singularities in the framework of particle trajectory crossing and vacuum occurrences, we will focus on this level of modeling in the present contribution.

The purpose of the present paper is to investigate the influence of second order schemes (centered versus upwind) on 2D structured deformed meshes as well as the level of discretization in space on the obtained results in two key configurations : 1- a simple stationary motor configuration with strong two-way coupling between the gas and the particle flow fields, where the coupling is responsible for two-phase losses prediction in SRM realistic configurations. This case is referred to as "TEP" and is a classical test-case in the literature.²³⁻²⁵ The configuration involves both difficulties with a singularity formation as well as vacuum occurrence; 2- an unsteady configuration of SRM called C1,²⁶⁻²⁸ involving the same difficulties, adds a hydrodynamical instability created by a sharp angle on the grain from what results thrust oscillations. The issues are robustness and accuracy of the methods in terms of transport in physical space for the condensed phase as well as the coupling with the gas; we would like to quantify their impact on the level of prediction of the models in both configurations. This issue has been partly investigated in Daniel et al.²⁹ However the recent progress in terms of numerical schemes (see³⁰ and references therein) as well as the recent analysis conducted on the mathematical structure of the equations requires a new analysis.

The paper is organized as follows. In Section 2, the global modeling strategy using a multi-fluid model with monokinetic assumption is presented, for the sake of generality in the polydisperse framework, even if we will then concentrate in this paper on monodisperse configuration in order to extract firm conclusions which are not blurred by

the polydisperse character of the spray. We emphasize the impact of the closure choices in terms of the properties of the model building blocks. Once the model established, the numerical strategy using operator splitting is presented as well as the key issue of discretizing the convective part of the Eulerian model for the condensed disperse phase. The chosen strategy in order to cope with potential singularities is highlighted since it will have a strong impact on robustness and accuracy. Section 4 is devoted to the TEP steady case analysis, whereas the unsteady C1 configuration is treated in section 5. In both cases, solutions are obtained using both CEDRE and SIERRA codes with different schemes. The conclusion of this work will then be proposed in order to provide intuitions about the impact, on the physical analysis, of the chosen numerical methodology to solve the governing equations. A strategy in order to obtain high accuracy, while preserving robustness will be especially highlighted.

2. Governing equations

In the present contribution, we focus on a fully Eulerian modeling of two-phase flows. We start from a coupled fluid-kinetic description of the coupling between a gaseous carrier flow and a moderately dense polydisperse spray of droplets/particles, which occupies a very small fraction of the total volume (disperse liquid phase, volume fraction below 1%). The purpose of this section is first to recall this fundamental modeling level, on which we can rely based on several previous studies. Then we highlight how a kinetic-based moment method (KBMM) for the disperse liquid phase, that is a presumed equilibrium velocity distribution conditioned in droplet size, can yield a two-way coupled system of conservation equations describing the two-phase flow. Since this is a cornerstone of fully Eulerian models, the mathematical structure and the potential occurrences of singularities are recalled at the end of the section.

2.1 Carrier phase model

For the carrier phase, we use the well known compressible Navier-Stokes equations for perfect gas under a 2D planar configuration. For the sake of legibility and clarity, the chosen form only considers a single component and a constant γ . We neglect the volume occupied by the disperse phase and the coupling between the phases is only taken into account through source terms, which will be identified more specifically in the next subsections. The resulting form of the system on the conservative vector $\mathbf{U}_g = (\rho, \rho u_{g,1}, \rho u_{g,2}, \rho E)^t$ reads :

$$\frac{\partial \mathbf{U}_g}{\partial t} + \frac{\partial \mathbf{F}_g}{\partial x_1} + \frac{\partial \mathbf{G}_g}{\partial x_2} = \mathbf{S}_g \quad \mathbf{F}_g = \begin{bmatrix} \rho u_{g,1} \\ \rho u_{g,1}^2 + \tau_{1,1} \\ \rho u_{g,1} u_{g,2} + \tau_{1,2} \\ (\rho E + \tau_{1,1}) u_{g,1} + \tau_{1,2} u_{g,2} - \lambda \frac{\partial T}{\partial x_1} \end{bmatrix} \quad \mathbf{G}_g = \begin{bmatrix} \rho u_{g,2} \\ \rho u_{g,1} u_{g,2} + \tau_{2,1} \\ \rho u_{g,2}^2 + \tau_{2,2} \\ \tau_{2,1} u_{g,1} + (\rho E + \tau_{2,2}) u_{g,2} - \lambda \frac{\partial T}{\partial x_2} \end{bmatrix} \quad (1)$$

where the source vector \mathbf{S}_g stand for the coupling with the disperse phase and requires a modeling choice, and \mathbf{F}_g and \mathbf{G}_g are the flux functions. The stress tensor $\underline{\underline{\tau}}$ is described through its components $\tau_{i,j} = P \delta_{i,j} - \mu \left[\frac{\partial u_{g,i}}{\partial x_j} + \frac{\partial u_{g,j}}{\partial x_i} - \frac{2}{3} \delta_{i,j} \frac{\partial u_{g,k}}{\partial x_k} \right]$.

Since it has been proved by Kourta in²⁸ that, in the case of a purely gaseous flow, the use of a URANS turbulent model does not significantly improve the results in the case of the typical configuration of solid propulsion we will investigate in the present paper, that is the C1 configuration, it has been chosen to conduct the simulations under a DNS context. Similar conclusions have been made for several LES turbulent models³¹ since only minor improvement have been observed in comparison with an axi-symmetrical experimental test case. In fact, turbulence spectrum of scale resolution as well as turbulence modeling are out of the scope of the present paper; since supersonic flows will be considered in the presence of boundary walls, since we do not want to impose very fine mesh close to boundaries especially in the nozzle and finally since the phenomenon to be resolved is driven by acoustic waves, walls have been chosen to be treated as frictionless boundaries. This will not restrict the scope of the study as we will see in the results and discussion section.

2.2 Disperse phase description

We will describe the polydisperse spray using a statistical description through a number density function, which satisfies a Williams-Boltzmann equation at the kinetic, also called mesoscopic, level. This allows to close the source terms in the gas phase equations as presented originally in Laurent et al.¹⁴ However, we envision a macroscopic level of description for the disperse phase, which relies on Eulerian moment methods and requires closure assumptions. Based on the kinetic theory of gases (see^{16,21} and references therein), we then derive a well-posed system of conservation equations modeling the disperse phase and provide the final source term coupling the two phases.

2.2.1 Kinetic description

The spray of aluminum oxide particles is represented through a number density function (NDF) f . The NDF depends on several parameters which are time, space, velocity, temperature (or enthalpy) and size (or mass). Its dynamics is described by the Williams-Boltzmann transport equation. It represents the evolution of the NDF of particles dispersed in a fluid allowing momentum exchange through a drag-force \mathbf{D}_F , thermal exchange H through convective or radiative terms and mass transfers R_S through vaporization and condensation. Assuming the statistical convergence through an infinite number of particles, the transport equation describing statistically the particle flow is given by :

$$f = f(t, \mathbf{x}, S, \mathbf{u}_p, T_p), \quad \underbrace{\partial_t f + \partial_{\mathbf{x}} \cdot (\mathbf{u}_p f)}_{\text{free transport}} + \underbrace{\partial_S (R_S f)}_{\text{evaporation}} + \underbrace{\partial_{\mathbf{u}_p} \cdot (\mathbf{D}_F f)}_{\text{drag force}} + \underbrace{\partial_{T_p} \cdot (H f)}_{\text{thermal transfert}} = \underbrace{\Gamma}_{\text{collision and break-up}} \quad (2)$$

where Γ is the integral operator describing particle-particle collisions, coalescence and break-up phenomena, S the size of the particle and T_p the temperature of the particles.

2.2.2 KBMM closure

Starting from this Eulerian description of the spray in a high dimensional phase space at mesoscopic scale, we aim at obtaining a system of conservation equations on moments at macroscopic scale. We will use a Kinetic Based Moment Method (KBMM) approach.²¹ It consists in assuming an equilibrium form of the NDF (as in kinetic theory), then following the evolution of the NDF only by observing mean statistical values called "moment" the dynamics of which are derived from Eq. (2). As for normal solutions of Boltzmann equations, there will always be a one-to-one correspondence between the moments and the equilibrium NDF at the mesoscopic level. One level of modeling in this hierarchy is given by the monokinetic assumption conditioned in size, with a specific form of the NDF:

[H1] At (t, \mathbf{x}) for a given droplet size S , there is only one velocity $\bar{\mathbf{u}}_p$ and the velocity dispersion is zero.

[H2] At (t, \mathbf{x}) for a given droplet size S , there is only one temperature \bar{T}_p and the temperature dispersion is zero.

$$f(t, \mathbf{x}, S, \mathbf{u}_p, T_p) = n(t, \mathbf{x}, S) \delta(\mathbf{u}_p - \bar{\mathbf{u}}_p(t, \mathbf{x}, S)) \delta(T_p - \bar{T}_p(t, \mathbf{x}, S)) \quad (3)$$

Where the droplet number density is the zeroth order moment defined by $n = \int f d\mathbf{u}_p dT dS$ and first order moment provide the velocity or temperature using the following formalism: $\forall \phi, n \bar{\phi} = \int \phi f d\mathbf{u}_p dT dS$. These two assumptions are fairly general for low inertia particles^{14,32} and we add a simplifying assumption for convenience and legibility of the present study, which will be conducted on monodisperse sprays:

[S3] The spray is assumed monodisperse everywhere at droplet size $\bar{S}(t, \mathbf{x})$, $n(t, \mathbf{x}, S) = n(t, \mathbf{x}) \delta(S - \bar{S}(t, \mathbf{x}))$.

More complex closure of the NDF allow to take into account polydispersity^{14,17,19} as well as dispersion in velocity.²¹ Obtaining conservation equations on moments up to order 1 is sufficient in order to close the system of equations because of hypotheses **[H1]**, **[H2]** and **[S3]**. By assuming that the enthalpy is a monotone function of the temperature $\bar{h} = h(\bar{T})$, the first order moment equation in temperature can be expressed under a more common form introducing the enthalpy. The system of conservation laws with source terms on the conservative spray variable $\mathbf{U}_p = (n, m, m \bar{u}_{p,1}, m \bar{u}_{p,2}, m \bar{h})^t$ then reads:

$$\frac{\partial \mathbf{U}_p}{\partial t} + \frac{\partial \mathbf{F}_p}{\partial x_1} + \frac{\partial \mathbf{G}_p}{\partial x_2} = \mathbf{S}_p \quad \mathbf{F}_p = \begin{bmatrix} n \bar{u}_{p,1} \\ m \bar{u}_{p,1} \\ m \bar{u}_{p,1}^2 \\ m \bar{u}_{p,1} \bar{u}_{p,2} \\ m \bar{h} \bar{u}_{p,1} \end{bmatrix} \quad \mathbf{G}_p = \begin{bmatrix} n \bar{u}_{p,2} \\ m \bar{u}_{p,2} \\ m \bar{u}_{p,2} \bar{u}_{p,1} \\ m \bar{u}_{p,2}^2 \\ m \bar{h} \bar{u}_{p,2} \end{bmatrix} \quad \mathbf{S}_p = \begin{bmatrix} 0 \\ 0 \\ m D_{F,x} \\ m D_{F,y} \\ m H \end{bmatrix} \quad (4)$$

For the sake of generality, the local diameter of the droplets is recovered from the two conserved quantities, number density n and mass density m through the relation $d_p = (6m)/(\rho_l \pi n)^{1/3}$. Knowing the diameters of the particles, the average drag forces $\bar{\mathbf{D}}_F = [D_{F,x} D_{F,y}]^t$ and heat exchange \bar{H} per unit of mass have analytic expressions in Stokes regime. For higher Reynolds number, the choice is oriented toward the classical correction of Schiller and Naumann for the drag force and the Ranz Marshall correction for heat exchange¹⁹ for instance, that are sufficient for SRMs applications. Source terms are then completely closed in terms of spray conservative variables and gas variables.

2.3 Gas-droplet interactions

Since the liquid disperse phase only occupies a negligible volume of the physical space, the two phase are transported independently in physical space, whereas they are coupled in the phase space through the source terms S_p . In order to take into account the backward action of the particles on the gas, the source term vector S_g has to be deduced from a global conservation in the system containing both gas and particles. Expressing the global conservation of momentum and heat allows to close S_g in the gas phase conservation equations (1): $S_g = [0; -m D_{Fx}; -m D_{Fy}; -m(H + \mathbf{D}_F \cdot \mathbf{u}_p)]^T$. Depending on the size of the particles and mass loading, this source term can be really stiff and brings in a strong coupling between the two phases.

2.4 Nature of equations

Once the global coupled model has been derived, it is natural to envision three blocks in the equations, which are related to transport in physical space for the gas \mathcal{T}_g , transport in physical space for the disperse liquid phase \mathcal{T}_p and transport in phase space for both phases, localized in physical space, through the global source terms \mathcal{S} . Such a decomposition is all the more natural since we will integrate the system in time using operator splitting.¹³ These blocks write :

$$\mathcal{T}_g \left\{ \frac{\partial \mathbf{U}_g}{\partial t} + \frac{\partial \mathbf{F}_g}{\partial x_1} + \frac{\partial \mathbf{G}_g}{\partial x_2} = 0 \quad \mathcal{T}_p \left\{ \frac{\partial \mathbf{U}_p}{\partial t} + \frac{\partial \mathbf{F}_p}{\partial x_1} + \frac{\partial \mathbf{G}_p}{\partial x_2} = 0 \quad \mathcal{S} \left\{ \begin{array}{l} \frac{\partial \mathbf{U}_g}{\partial t} = S_g(\mathbf{U}_g, \mathbf{U}_p) \\ \frac{\partial \mathbf{U}_p}{\partial t} = S_p(\mathbf{U}_g, \mathbf{U}_p) \end{array} \right. \quad (5)$$

These operators have different natures. The source term \mathcal{S} is constituted of a set of decoupled ODEs parametrized by space location, while \mathcal{T}_g and \mathcal{T}_p are PDEs depending on time and space, even if uncoupled. If the Navier-Stokes equations, described by \mathcal{T}_g , have well known mathematical properties (mixed hyperbolic-parabolic), the mathematical characteristics of the Pressureless Gas Dynamics equations contained in \mathcal{T}_p are less identified but highly relevant, in such a way that we need to shed some light on some key issues. More specifically the operator \mathcal{T}_p has several properties:

Maximum principle The velocity remains bounded between its original minimal and maximal values.^{32,33} Then the solution lives, relatively to the velocity, in a bounded domain. This stability property is going to be a strong advantage compared to Euler equations for example in order to build stable numerical schemes and in order to check the consistency of the results. More generally, every other transported quantity of the system satisfies a maximum principle (see also Emre et al.¹⁶ and references therein), that includes \bar{h} and n/m . Moreover, we also have a maximum principle on number density and temperature, which guarantees realizability for number density, mass density and temperature, that is they remain positive everywhere and are thus the moments of some distribution function. These mathematical properties should be satisfied by any numerical approximation of the solution.

δ -shock In general, the mathematical solution of the PGD equation can lead to solutions including Dirac delta functions in density, called δ -shocks. The monokinetic assumption is the source of that phenomenon and fails interpreting the microscopic behavior through macroscopic variables in case of inertial particles and PTC,³² since only the average velocity is represented. In such a situation a higher order moment method in velocity should be used²¹; this can be considered as a drawback of the Eulerian modeling of the particles, which has to adapt locally to various order of moment methods. Once again, these models are not presented here since the choice has been made to keep a commonly used system of equations with typical difficulties encountered in SRM modeling and simulation.

vacuum When considering the volume density of droplets, vacuum zones are common in two-phase flow. They can be the result of the injection process, where no droplets are injected in some regions or can be created since a drift velocity exists between gas and particles through inertia in vortical flows. Besides, because of the inertia of the droplets, vacuum zones usually appear in the divergent of the nozzle. Since the conservative variables are equal to zero in these conditions, several deduced values such as velocity or diameter remain undefined. Whereas such zones are perfectly defined at the continuous level, they will prove to be hard to deal with in the numerical discretization of the equations, all the more since density has to remain positive, even in zone where the density can be very close to zero, thus forbidding any oscillatory behavior.

3. Numerical methods

The purpose of this section is to expose the general numerical strategy, which will be used in the results and discussion sections. After recalling the fundamentals of Strang operator splitting, which allows to decouple transport in physical

space for gas and liquid from the resolution of their coupling in the source term, we will present the choices in terms of both integration of transport in physical space for gas and liquid and then dynamics in phase space through source terms integration. Let us underline that the main subject of the further presented analysis is related to the transport in physical space for both phase, with special emphasis on the liquid phase; in these matters, we will focus on explicit schemes for unsteady problems with supersonic flows and acoustics resolution.

3.1 Strang scheme and source time integration

We use Strang operator splitting (see Doisneau et al^{13,34} and references therein since this is not the main contribution of this paper). Denoting $\mathcal{R}^{\Delta t}U(t)$ the resolution of operator \mathcal{R} during a time step Δt starting for a value $U(t)$, the Strang scheme used to couple the global system is then expressed under the following form :

$$U^{Strang}(t + \Delta t) = S^{\Delta t/2}[\mathcal{T}_g^{\Delta t}\mathcal{T}_p^{\Delta t}]S^{\Delta t/2}U(t) \quad (6)$$

The splitting time step Δt will be chosen in the configurations encountered in the proposed test-cases to be related to the CFL condition for the carrier phase transport in physical space explicit integration, which is related to acoustic wave resolution. Assuming the possibility of stiff source, the integration of the source has to be treated with care, either with explicit or implicit methods. For the cases we will present, an explicit integration of the source terms using the splitting time step will be stable. Let us nonetheless emphasize that the two time steps (splitting time step and source integration time step) do not need to be the same. The integration of ODEs, i.e. the operator S , is standard and will rely on a usual Runge-Kutta procedure of order three respecting the SSP properties.³⁵ This version of explicit Runge-Kutta method has been revealed to be robust in many situations.²⁷

3.2 Transport schemes

We will use a finite volume approach on 2D structured deformed meshes and on their unstructured meshes counterparts. Two classes of scheme, centered and upwind, will be considered for the integration of the transport in physical space of both gas and liquid. In order to use common notations for both \mathcal{T}_g and \mathcal{T}_p , the formalism used in Eq. (5) is kept. The integration of the transport operators over a control volume Ω representing the cell is given by :

$$\iiint_{\Omega} \frac{\partial U}{\partial t} = - \oint_{S_{1to4}} [(\mathbf{F}\vec{i} + \mathbf{G}\vec{j}) \cdot \vec{n}] dS \quad (7)$$

where \vec{i} and \vec{j} are respectively the unit vectors of the axis x_1 and x_2 , \vec{n} the normal to the face S of the cell assuming there are four faces because of the 2D structured deformed framework.

3.2.1 Centered schemes

Originally used in the framework of finite differences, most of centered schemes can generally be expressed under a finite volume framework thanks to their conservation property. They are known to be subject to oscillations close to large gradients and discontinuities, but thanks to their numerical efficiency and accuracy in smooth cases, these schemes have been widely used. The method implemented in the in-house SIERRA code, originally used by ONERA in the 90's for transport of both gas and particles in SRMs context, is based on a MacCormack scheme.³⁶ Based on a predictor-corrector procedure, it can deal with hyperbolic PDE and only flux function calls are required. Intrinsically linked to a structured grid, the indexes of position i and j are introduced in its formulation:

$$\begin{cases} \widetilde{U}_{i,j}^{n+1} = U_{i,j}^n - \Delta t \sum_{k=4 \text{ sides}} \left\{ \mathbf{F}_k^{\pm} \frac{S_k}{V(i,j)} \vec{i} \cdot \vec{n} + \mathbf{G}_k^{\pm} \frac{S_k}{V(i,j)} \vec{j} \cdot \vec{n} \right\}^n \\ U_{i,j}^{n+1} = \frac{1}{2} \left[U_{i,j}^n + \widetilde{U}_{i,j}^{n+1} - \Delta t \sum_{k=4 \text{ sides}} \left\{ \mathbf{F}_k^{\mp} \frac{S_k}{V(i,j)} \vec{i} \cdot \vec{n} + \mathbf{G}_k^{\mp} \frac{S_k}{V(i,j)} \vec{j} \cdot \vec{n} \right\}^{n+1} \right] \end{cases} \quad (8)$$

where n is used to indicate the original step, $n+1$ the predictor step, S_k the surface of the side k of the cell, \pm the side chosen for flux computation and $V(i, j)$ the volume of the cell.

The predictor is estimated through the flux function from one side of the surface S_k and the corrector used the flux function from the other side of this same surface in order to increase the accuracy. Because of the globally known flow orientation, it has been chosen to use a predictor upstream oriented, in other words, toward the grain for the

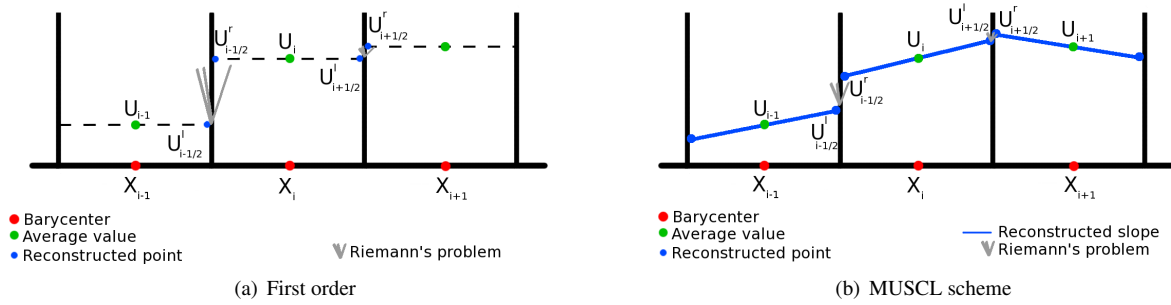


Figure 1 – Sub-cell distribution for upwind scheme

horizontal faces and toward the head-end for the vertical faces. Artificial Viscosity (AV) is then added in order to improve the results and stabilize the solution by tackling intrinsic spurious oscillations. It consists in adding a blending of second-difference and fourth-difference dissipation terms close to high gradients detected by a sensor in order to preserve the smooth part from any additional diffusion. The methodology used by Jameson and Baker³⁷ is chosen for this issues but since the original sensor is based on pressure, this procedure cannot be directly applied on the transport of particles. As a consequence, density is used as the sensor variable of \mathcal{T}_p while the pressure is kept for \mathcal{T}_g .

3.2.2 Upwind scheme

Whereas centered schemes solve hyperbolic PDEs through the computation of the flux function at the barycenter of a cell, upwind schemes aim at solving Riemann problems discontinuities at faces. This kind of method can reach higher order through the reconstruction of the resolved field inside the cell.

This original idea of first order Godunov scheme is to resolve a 1D Riemann problems at each cell interface in the normal direction. Since the solution of the Riemann problem remains constant in time at the cell face, the numerical flux between both cells is deduced from that value. In the case of Navier-Stokes equations, the resolution of the exact Riemann solution can be costly since it requires an iterative procedure. That explains the highly studied subject of approximate Riemann solvers³⁸ in order to increase the numerical efficiency resulting for instance in the HLLC solver use for gas in the conducted CEDRE simulations. However, the PGD equations have an explicit solution to the Riemann's problem.³³ Then, this exact Riemann solver is chosen for the disperse phase resolution. Denoting U_k^* the solution of the Riemann problem at the face k , the scheme takes the following expression:

$$U_{i,j}^{n+1} = U_{i,j}^n + \frac{\Delta t}{V(i,j)} \sum_{k=4 \text{ sides}} [S_k(F(U_k^*) + G(U_k^*))] \quad (9)$$

The previously described strategy is first order since the values used at the interfaces of the cells are the average values. Assuming the possibility of an affine reconstruction of the solution in the cells, more accurate values are reconstructed at the faces. Introduced by Van Leer³⁹ under the name of MUSCL, a graphical representation of the method principle is given in Figure 1. Using reconstruction respecting Total Variation Diminishing (TVD) properties, this scheme has been proven to be both robust and accurate even through discontinuities.

The MUSCL method in a multidimensional context depends on the interpretation of the scheme. Usually, a gradient over the cell is computed thanks to the neighbors ones.⁴⁰ A long term development has been conducted for the CEDRE gas solver for such schemes providing very reliable results.

However the development of robust and accurate schemes for eulerian particle simulation requires some special effort due to the structure of the system of conservation equations. Recent development at ONERA have been undertaken in order to obtain a maximal accuracy within the framework of a MUSCL method, while maintaining robustness through a maximum principle on velocity and density in order to reach robustness and realizability. This methodology defined as multislope³⁰ proposes a projection of the values on a well oriented axis in order to only cope with a one dimensional framework. Mathematically proved to be L_∞ stable, it has been revealed to be both more robust and accurate than the classical multi-dimensional MUSCL formulations for unstructured mesh while being more efficient.

The second order upwind scheme described above is of order two in space but not in time. The procedure is then complement by a time integration using the explicit Runge-Kutta method of order two that respects the Strong Stability

Preserving (SSP) properties,³⁵ also known as Heun scheme. This procedure is not needed for the MacCormack scheme since it is already of order two in space and time. Gaseous phase resolution in CEDRE also includes implicit time resolution thus inducing a less restrictive CFL and therefore a larger time step in order to reduce the computational cost. Let us underline that stability of implicit schemes does not induce accuracy.

The MUSCL definition expressed above has been originally designed for linear advection and the resolution of more complex system of equations brings in the freedom of choosing the variables of reconstruction. If it is easier to choose the conservative variables, this solution appears not to be the most reliable. The choice of primitive variables is especially suited for the equations of the disperse phase since it has been shown to lead to a discrete maximum principle property on the velocity in the framework of structured cartesian meshes and kinetic schemes.¹⁵ Even if it is beyond the scope of the present paper, it can be proved that the proposed strategy leads to a discrete maximum principle property on general unstructured meshes and deformed structured meshes under proper CFL condition.

In the context of upwind schemes, a TVD reconstruction can be seen as a reconstruction that does not create artificial extrema through its procedure. Moreover the resolution of the numerical flux can prevent creating new extrema, relatively to the reconstructed values, if a maximum principle is given. The combination of both properties results in guaranteeing that the reconstructed variables stay in the expected bounds. Similarly, applying this same principle on the density or particle number resulting in preventing these values to be negative since they respect a minimum principle. However the separated reconstruction of the mass density and the particle number density does not prevent the change of particle size during the reconstruction procedure. Inspired from the works related to higher size moment methods for representation of polydisperse particle flow,^{16,17} it is chosen to reconstruct the solution using m and n/m , instead of m and n separately, and results in a second order accurate scheme that preserves realizability.

3.3 An industrial code CEDRE and an in-house code SIERRA

The simulations presented hereafter are conducted using two codes. The in-house code SIERRA solves the carrier phase conservation equations through a MacCormack scheme with a low level of AV, on 2D structured deformed meshes. The disperse phase is resolved either using a centered scheme or an upwind scheme (either first or second order) in order to compare the impact of such a choice. In that context, the second order AV coefficient $\kappa^{(2)}$ of the MacCormack scheme is one order of magnitude larger than the one used for the gaseous flows field²⁷ for stability issues. The fourth order AV coefficient $\kappa^{(4)}$ has to be taken as zero since it is incompatible with the vacuum zones naturally present in the studied configurations and leads to unstable behaviors. The recent developments of explicit multislope MUSCL upwind schemes³⁰ have been implemented in SIERRA for the resolution of the disperse phase. They are the same as their counterpart implemented in the industrial CEDRE code developed at ONERA on fully unstructured meshes. Whereas the gaseous flow field is resolved using centered schemes in SIERRA, upwind schemes of multislope MUSCL type are used in CEDRE, either explicit or implicit. For the purpose of comparing the results obtained with the two codes, the meshes will be the same for all SRM simulations, that is deformed structured meshes, even if treated in terms of different data structures in the two codes.

4. Steady TEP simulation

We will first focus on a simplified SRM configuration TEP that produces, despite its simple geometry, several levels of singularities typical of what will be encountered in realistic SRM simulations. Usually, the TEP geometry corresponds to a cylindrical port motor of chamber length 170 mm and inner radius 45 mm continued by a converging-diverging nozzle of throat radius 16.77 mm for an overall motor length of 270 mm (see Figure 2). Here, the simulations will be conducted in a 2D-planar configuration with the gas and particle properties provided in Table 1. Presenting no difficulty for full gaseous simulations,²³ the numerical method used for solving the carrier phase flow will have a negligible influence on the results. However, complications occur for two-phase flows^{24,25} resulting in the need of an adaptation of the AV as explained above. The discussion will be oriented toward the resolution of the delta-shock and of the interface with vacuum, which turns out to be the most critical area relatively to scheme behavior; the impact of mesh refinement in the presence of such singularities will then be investigated.

4.1 Resolution of singularities and vacuum

Due to the compression of the flow in the nozzle inlet, trajectories of the particles originating from the aft-end part of the grain encounter the path of the particles coming from the head-end and flowing downstream. The physical PTC occurring even for such low inertia particles results in a mathematical δ -shock with a position that depends on the numerical method used for the resolution of the disperse phase. For instance, the first order scheme produces a δ -shock

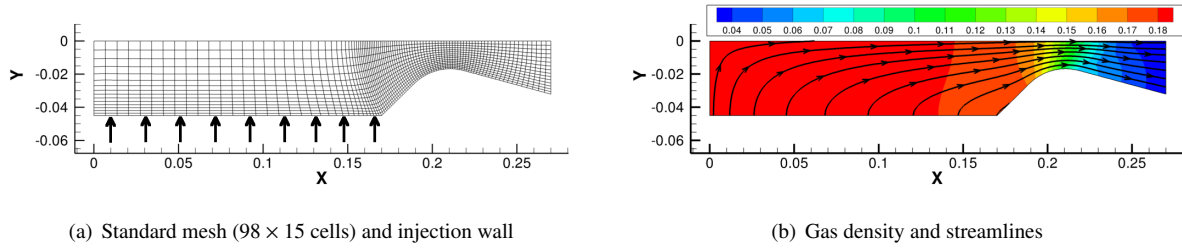


Figure 2 – TEP configuration representation

Table 1 – gas and particle properties for the TEP test case

Gas	Value	Gas	Value	Droplets	Value	Droplets	Value
γ	1.14	\dot{m}_g	$11.4 \text{ Kg/m}^2/\text{s}$	ρ_p	1803 Kg/m^3	\dot{m}_p	$0.6 \text{ Kg/m}^2/\text{s}$
$C_{p,g}$	2437.1 J/Kg/K	μ	$7.95 \times 10^{-4} \text{ Pa} \cdot \text{s}$	$C_{p,p}$	1419 J/Kg/K	$V_{p,inj}$	1 m/s
T_0	3387 K	Pr	1	$T_{p,0}$	3387 K		

attached to the nozzle inlet wall (see Figure 3) while the same δ -shock is solved detached from it using higher order schemes. Moreover because of the numerical diffusion related to the scheme used, the position and the amplitude of the shock can change moving toward the chamber under the effect of diffusion.

The drift velocity due to the inertia of the particles naturally produces a vacuum zone in the diverging part of the nozzle. Moreover, since the δ -shock prevents any PTC, vacuum naturally appears right behind it, thus creating an especially high gradient that the numerical methods have to cope with. The centered scheme are challenged in such a condition since intrinsic spurious oscillations appear and can easily lead to negative density close to vacuum. The AV then has a high impact on the resolution in such an area. However, since the first order upwind scheme and the MUSCL scheme are intrinsically designed to avoid negative density, no numerical artifact resulting from the interface with vacuum can be observed. The width of the transition zone from vacuum to the δ -shock depends however on the level of numerical diffusion. In the present case, the widest zone is observed for the first order Godunov scheme, the thinnest for the MUSCL scheme. For the MacCormack scheme, this width highly depends on the AV parameters.

4.2 Influence of mesh refinement on the results

If differences are expected from the approximation of a mathematical solution by several methods, successive mesh refinements should lead to a unique solution. However, singularities occurring in the TEP assesses the ability of the methods to provide the correct solution. Aside the more accurate resolution of the particle flow, the finer resolution of the carrier phase reveals small structures, naturally occurring and taking place at the head end on the symmetry plane and at the junction between the injection surface and the nozzle. These lower scale structures lead to physical stagnation points and therefore droplet accumulations that challenge even more the centered schemes.

Since the gradients increase with mesh refinement, the second order artificial viscosity coefficient has to be increased to prevent the simulation from diverging. The use of the minimal amount of artificial viscosity for stability leads to oscillations similar to those already observed with the standard mesh as in Figure 4. A high increase of the AV in order to reduce these wiggles actually leads to more intense oscillations. As a consequence, even if an optimal level of AV can be reached, the MacCormack scheme, in this standard form and using this kind of AV, does not allow to get rid of the oscillating fields and requires tedious manual adjustment in order to reach a satisfactory solution.

In contrast, the upwind class of schemes does not need artificial viscosity nor case dependent corrections. For the first order scheme, it can be seen that high mass accumulations occur at the head-end of the engine and near the symmetry plane. These artificial singularities are limited to the boundary cells where δ -shocks are actually created through diffusion. Using a MUSCL second-order extension, these numerical singularities disappear and effective mass accumulations due to stagnation points are revealed. Observing the transition zone to vacuum, even if refined meshes yield a thinner zone with first order scheme, the use of the MUSCL scheme is much more efficient in reducing the spreading of the zone due to numerical diffusion. Comparing the accuracy of the solution obtained at comparable computational cost, the effort conducted in order to get a stable and accurate second order extension is then fully justified

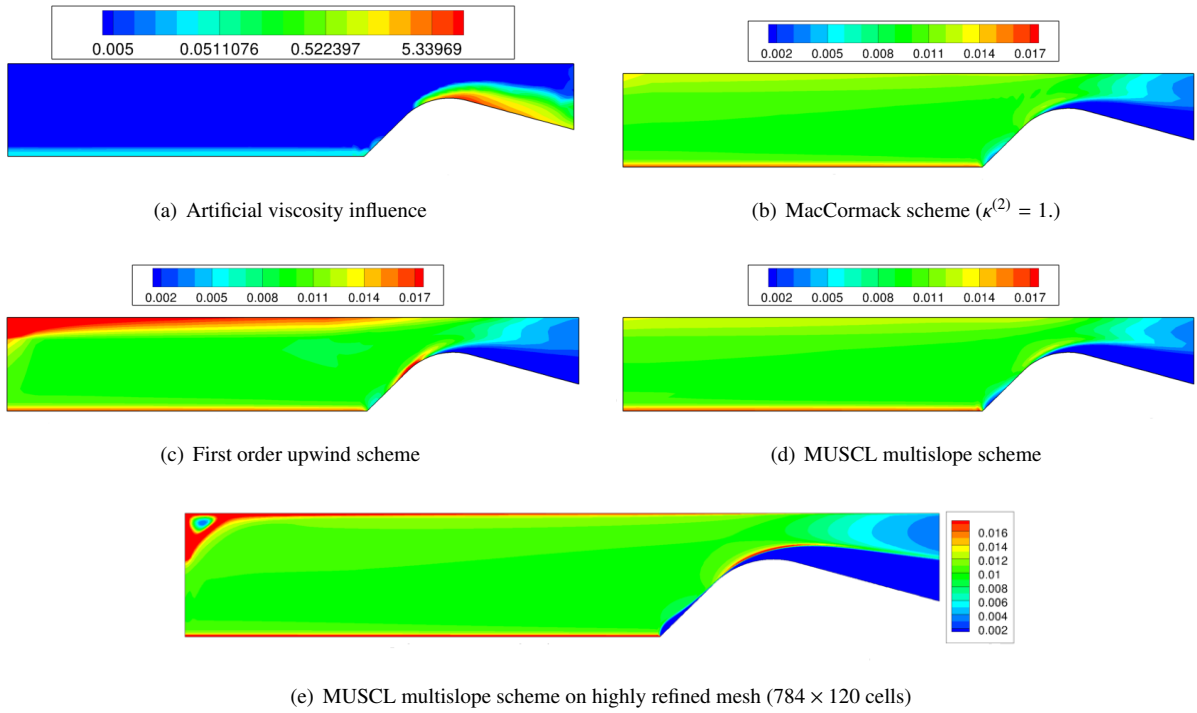


Figure 3 – Influence of the scheme on the density field resolution for TEP case

since the MUSCL scheme can provide more accurate results on coarser meshes than the first order method.

Because of the singularity formation, usual notions such as convergence have to be investigated beyond smooth flows. The design of a specific scheme is needed in order to resolve both vacuum zones and δ -shock but more importantly to obtain coherent solutions in every configurations. Consequently, applying a mesh refinement without tackling these issues can lead to unexpected phenomena and the false interpretation of numerical effects. Eventually, the proposed upwind scheme which combines accuracy and stability allows to conduct a proper mesh refinement study without any inference from parameters, which are difficult to control.

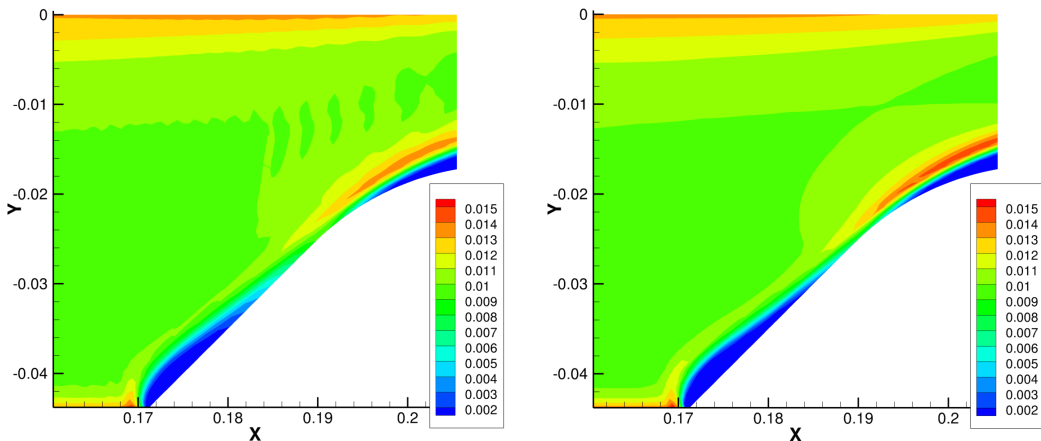


Figure 4 – Droplet density field in the converging part of the nozzle for TEP refined mesh (196×30 cells) using MacCormack scheme (left) and MUSCL multislope scheme (right)

5. Unsteady test case simulation

Keeping in mind the previous issues, the study of the C1 unsteady configuration will point out other phenomena and quantify the impact of the numerical method chosen on pressure oscillation occurring inside this fictive SRM with low inertia particles, which is representative of realistic SRM configuration. Finally thanks to a well chosen size of more inertial particles, it will be possible to investigate the impact of the scheme accuracy and stress the importance of an accurate particle field resolution.

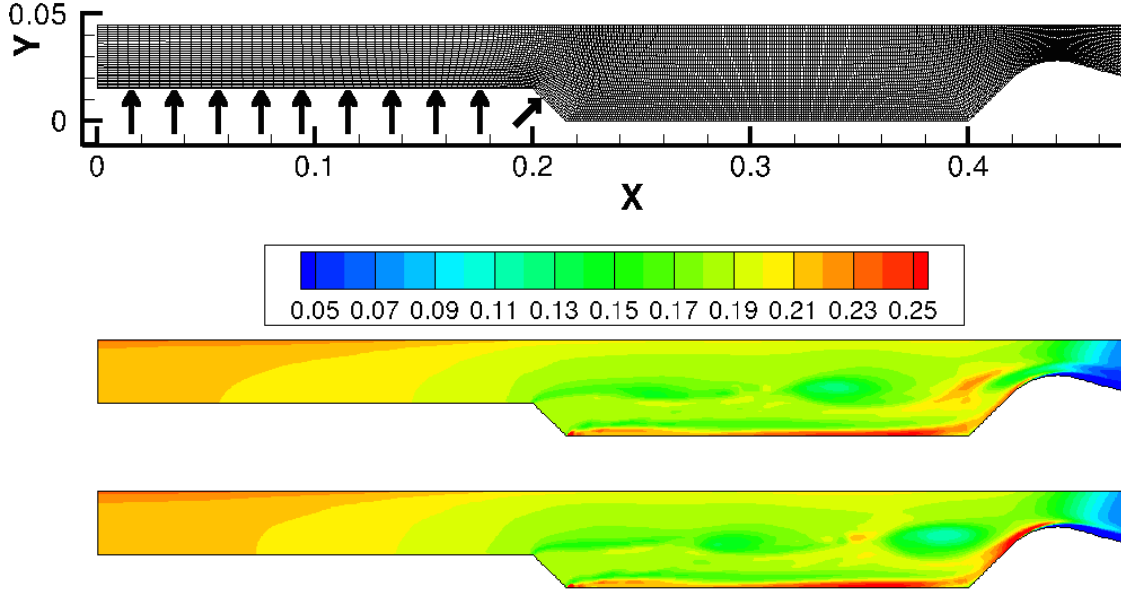


Figure 5 – C1 mesh (top) and particle density field evolution at times $t = 0 \mu s$ (middle) and $t = 220 \mu s$ (bottom)

The C1 test case corresponds to the internal geometry of a motor built to favor a vortex shedding phenomenon inside the chamber. To achieve this, the injected surface is located in the first half of the chamber and interrupted by a sharp edge. This configuration gives rise to a flow induced excitation coupled to the acoustics of the chamber, essentially the second longitudinal mode, and called VSA for Vortex Shedding of Angle. The test case assumes a 2D-planar geometry. The configuration was originally designed for single phase flow,^{28,41} then extended to the study of two-phase flow^{26,27} with properties given in Table 2 and mesh given in Figure 5.

Since unsteady acoustic phenomena are the main issues under investigation, a high temporal resolution is needed, which induces small time steps. A long integration time and a high number of iterations are also required in order to draw some firm conclusions on the frequency analysis of the observed periodic flows, which justify to some extent the size of the considered meshes. According to Morfouace and Tissier²⁶ one can find a main frequency of $2650 Hz$ for the gas alone and $2250 Hz$ for a flow loaded with $5 \mu m$ particles. Using $16 \mu m$ particles (for which the acoustic Stokes number defined as the ratio of particle relaxation time to the acoustic time⁴² is close to one), oscillations are totally damped, revealing the impact of the size of the disperse phase particles on the physics in such configurations.

5.1 Unsteady behavior with $5 \mu m$ particles

The impact of $5 \mu m$ particles has already been studied and analyzed.^{26,27} In the present study, a monochromatic signal on the head-end pressure sensor is obtained in accordance with previous works. Various schemes and refinement

Table 2 – Gas and particle properties for the C1 test case

Gas	Value	Droplets	Value				
γ	1.14	\dot{m}_g	$21.201 \text{ Kg/m}^2/s$	ρ_p	1766 Kg/m^3	\dot{m}_p	$8.3956 \text{ Kg/m}^2/s$
$C_{p,g}$	2439.03 J/Kg/K	μ	$3.6 \times 10^{-4} \text{ Pa} \cdot s$	$C_{p,p}$	1375 J/Kg/K	$V_{p,inj}$	$= V_{g,inj}$
T_0	3387 K	Pr	1	$T_{p,0}$	3387 K		

Table 3 – Head end pressure signal for the $5\mu\text{m}$ particle configuration

Scheme for: \mathcal{T}_p	\mathcal{T}_g	Main frequency	$\sqrt{2}RMS$ (mbar)
Standard Mesh	(317 × 30)		
First order	MacCormack	$2089 \pm 6 \text{ Hz}$	19.45
MacCormack	MacCormack	$2141 \pm 6 \text{ Hz}$	33.91
Multislope	MacCormack	$2153 \pm 6 \text{ Hz}$	33.63
Multislope	Multislope ^a	$2165 \pm 7 \text{ Hz}$	24.34
Multislope	Multislope ^b	$2173 \pm 7 \text{ Hz}$	19.73
Multislope	Multislope ^c	$2173 \pm 7 \text{ Hz}$	16.87
Refined Mesh	(634 × 60)		
First order	MacCormack	$2129 \pm 6 \text{ Hz}$	25.14
MacCormack	MacCormack	$2165 \pm 6 \text{ Hz}$	32.45
Multislope	MacCormack	$2171 \pm 6 \text{ Hz}$	35.12
Multislope	Multislope ^a	$2165 \pm 15 \text{ Hz}$	32.72
Multislope	Multislope ^b	$2157 \pm 10 \text{ Hz}$	31.26

^a Explicit RK2 time integration using CEDRE

^b Implicit RK1 time integration using CEDRE and twice larger time step

^c Implicit RK1 time integration using CEDRE and three time larger time step

levels, as presented in Table 3, are assessed on this challenging configuration. The methods give coherent results but differences exist and mostly depend on the diffusion induced by the schemes on both gas and particles. To reduce the computation cost, two strategies have been used: 1- an implicit time step on the gas can be used, however it reduces the oscillation amplitude but accurately resolves the acoustic wave velocity, 2- a first order scheme on the droplet flow, which smears out the oscillation and introduces a shift in frequency in the same time. As instabilities are coupled to the acoustics of the chamber, it is possible to compare the ratio of the two-phase to single-phase oscillation frequencies to the theoretical ratio of the sound propagation speed in a homogeneous two-phase medium to the one in a pure gas, as explained for instance in.⁴² With data provides in Table 2, the second ratio is 0.836, while simulations yield a first ratio of 0.83 for the more accurate simulations and about 0.81 for the first order scheme on the refined mesh. Consequently, it can be observed that the heterogeneous spatial repartition of the particles, even if better resolved by the most accurate schemes, have less influence on the speed of sound than the dispersive character of the first order scheme. Second order explicit methods for both gas and particles are necessary in order to obtain predictive results on relatively coarse space discretizations.

The MUSCL scheme used for the transport of particles respects TVD properties. It is thus first order at extrema which lowers the oscillation amplitude obtained in the CEDRE simulations. However, the solution quickly converges through mesh refinement to the values obtained using the MacCormack scheme for gas. Let us highlight that in the context of the MacCormack scheme used for particles, the increase of the AV for stability issues leads to an increase of the numerical diffusion and thus to a slight reduction of the oscillation amplitude through the refined mesh. Considering this behavior and the need to increase even more the AV while refining the mesh, such as in the TEP test case, the ability of this numerical strategy to produce more accurate result on such configuration is not ensured.

5.2 Instability development for $20\mu\text{m}$ particles

In order to discriminate the sensitivity of the methods, simulations with $20\mu\text{m}$ particles have been conducted corresponding to a limit between a steady and an unsteady configurations close to a bifurcation point. The detection of a VSA phenomenon can be obtained using accurate schemes and/or refined mesh (see Table 4). Only the less diffusive scheme, with multislope method for particles and a MacCormack scheme for the carrier phase, is able to detect an instability on the standard mesh. However the amplitude observed is highly lowered compared to the results obtained through mesh refinement, which also reveals a shift of the main frequency from 2121 Hz to 1463 Hz . Such a mode does not match with any acoustic mode of the chamber. The accurate resolution of the problem through a highly refined mesh using the CEDRE code confirms this tendency but it has to be highlighted that in both cases the signal observed is no more monochromatic. Since no other results are available in the literature for this specific size of particles, further investigation are needed in order to draw definite conclusion in that case. However, this case points out the robustness and accuracy of the proposed scheme to detect instabilities on coarse and refined spatial discretization even if a finer resolution is still needed in order to obtain fully converged results.

Table 4 – Head end pressure signal for the 20 μ m particle configuration

Scheme for: \mathcal{T}_p	\mathcal{T}_g	VSA detection	Main frequency	$\sqrt{2}RMS$ (mbar)
Standard mesh	(317 \times 30)			
First order	MacCormack	no	-	-
MacCormack	MacCormack	no	-	-
Multislope	MacCormack	yes	2121 \pm 16 Hz	0.2625
Multislope	Multislope ^a	no	-	-
Refined mesh	(634 \times 60)			
First order	MacCormack	no	-	-
MacCormack	MacCormack	no	-	-
Multislope	MacCormack	yes	1463 \pm 13 Hz	17.8
Multislope	Multislope ^a	yes	2173 \pm 13 Hz	6.21
Highly refined mesh	(1268 \times 120)			
Multislope	Multislope ^a	yes	1430 \pm 35 Hz	5.57

^a Explicit RK2 time integration using CEDRE

6. Conclusion

The presented contribution has investigated two categories of schemes, namely centered and upwind, on two SRM test configurations. The ability of the MUSCL schemes used, such as implemented in the CEDRE software, to produce accurate and reliable solution have been proved to be a key point, in the conducted simulations, to reach predictable solution. On the contrary, despite its high accuracy in smooth configurations, the MacCormack scheme requires a very specific adjustment of the AV that does not ensure the quality of the result obtained. Such problem could be solved through a TVD-MacCormack method⁴³ but has not been studied in the present paper. Moreover, the investigation of the unsteady case stressed the importance of the accurate resolution of the disperse phase in order to predict properly the onset of instability and more generally the behavior of the solid rocket engine such as its performances at a reasonable cost. Finally the sensitivity of the flow to the size of aluminum oxide droplets points out the importance of the treatment of size polydispersion in industrial configurations.

Acknowledgments

The present research was conducted thanks to a Ph.D. Grant from ONERA. This work relies on a long-term collaboration work between EM2C laboratory and the Fundamental and Applied Energetics (DEFA) department at ONERA. We would like to thank E. Radenac for providing us with the very helpful numerical tools used for acoustic analysis.

References

- [1] R. F. Hoglund, "Recent advances in gas-particle nozzle flows," *ARS Journal*, vol. 32, no. 5, pp. 662–671, 1962.
- [2] R. W. Hermsen, "Aluminum oxide particle size for solid rocket motor performance prediction," *Journal of Spacecraft and Rockets*, vol. 18, no. 6, pp. 483–490, 1981.
- [3] E. W. Price, "Experimental observations of combustion instability," in *Fundamentals of Solid-Propellant Combustion*, vol. 90 of *Progress in Astronautics and Aeronautics*, pp. 733–790, AIAA, 1984. Edited by K. K. Kuo and M. Summerfield.
- [4] F. E. C. Culick and V. Yang, "Prediction of the stability of unsteady motions in solid-propellant rocket motors," in *Nonsteady Burning and Combustion Stability of Solid Propellants*, vol. 143 of *Progress in Astronautics and Aeronautics*, pp. 719–779, AIAA, 1992. Edited by L. de Luca, E. W. Price and M. Summerfield.
- [5] R. S. Brown, R. Dunlap, S. W. Young, and R. C. Waugh, "Vortex shedding as a source of acoustic energy in segmented solid rockets," *Journal of Spacecraft and Rockets*, vol. 18, no. 4, pp. 312–319, 1981.
- [6] F. Vuillot, "Vortex-shedding phenomena in solid rocket motors," *J. Propulsion and Power*, vol. 11, no. 4, pp. 626–639, 1995.

- [7] N. Lupoglazoff and F. Vuillot, "Parietal vortex shedding as a cause of instability for long solid propellant motors - Numerical simulations and comparisons with firing tests," in *34th AIAA Aerospace Sciences Meeting and Exhibit*, AIAA Paper 96-0761, pp. 1-10, January 1996. Reno, NV.
- [8] G. Casalis, G. Avalon, and J.-P. Pineau, "Spatial instability of planar channel flow with fluid injection through porous walls," *Physics of Fluids*, vol. 10, no. 10, pp. 2558-2568, 1998.
- [9] M. W. Beckstead, "Evidences for distributed combustion," in *Proceedings of the 24th JANNAF Combustion Meeting*, vol. 1, pp. 1-12, 1987.
- [10] S. Gallier and F. Godfroy, "Aluminum combustion driven instabilities in solid rocket motors," *Journal of Propulsion and Power*, vol. 25, no. 2, pp. 509-521, 2009.
- [11] P. Kuentzmann, "Instabilités de fonctionnement des systèmes propulsifs," *La Recherche Aéronautique*, vol. 5, pp. 341-351, 1995.
- [12] J. Dupays, F. Godfroy, O. Orlandi, P. Prevot, M. Prévost, S. Gallier, S. Ballereau, and Y. Fabignon, "Inert condensed phase driving effect of combustion instabilities in solid rocket motor," in *5th International Spacecraft Propulsion Conference*, pp. 1-8, May 2008. Heraklion, Greece.
- [13] F. Doisneau, A. Sibra, J. Dupays, A. Murrone, F. Laurent, and M. Massot, "Numerical strategy for unsteady two-way coupled polydisperse sprays: application to solid-rocket instabilities," *Journal of Propulsion and Power*, vol. 30, no. 3, pp. 727-748, 2014.
- [14] F. Laurent and M. Massot, "Multi-fluid modeling of laminar poly-dispersed spray flames: origin, assumptions and comparison of the sectional and sampling methods," *Comb. Theory and Modelling*, vol. 5, pp. 537-572, 2001.
- [15] M. Massot, *Eulerian Multi-Fluid models for polydisperse evaporating sprays*, ch. III of "Multi-Phase Reacting Flows: Modelling and Simulation", pp. 79-123. CISM Courses and Lectures No. 492, Springer, 2007. Editors D.L. Marchisio and R. O. Fox.
- [16] O. Emre, D. Kah, S. Jay, Q.-H. Tran, A. Velghe, S. De Chaisemartin, R. Fox, F. Laurent, and M. Massot, "Eulerian moment methods for automotive sprays," *Atomization and Sprays*, vol. 25, pp. 189-254, 2015.
- [17] F. Laurent, A. Sibra, and F. Doisneau, "Two-size moment Eulerian Multi-Fluid model: a flexible and realizable high-fidelity description of polydisperse moderately dense evaporating sprays," *Submitted, Communication in Computational Physics*, pp. 1-42, 2015. HAL: <https://hal.archives-ouvertes.fr/hal-01169730/en>.
- [18] F. Doisneau, F. Laurent, A. Murrone, J. Dupays, and M. Massot, "Eulerian Multi-Fluid models for the simulation of dynamics and coalescence of particles in solid propellant combustion," *Journal of Computational Physics*, vol. 234, pp. 230-262, 2013.
- [19] A. Sibra, J. Dupays, A. Murrone, F. Laurent, and M. Massot, "Simulation of reactive sprays coupled to unsteady flows in solid rocket motors: Efficient strategy using Eulerian Multi-Fluid methods," *Submitted to Journal of Computational Physics*, pp. 1-41, 2014. HAL: <https://hal.archives-ouvertes.fr/hal-01063816>.
- [20] C. Chalons, R. O. Fox, and M. Massot, "A multi-Gaussian quadrature method of moments for gas-particle flows in a LES framework," *Summer Program Proceedings, Center for Turbulence Research, Stanford University*, pp. 347-358, 2010.
- [21] A. Vié, F. Doisneau, and M. Massot, "On the Anisotropic Gaussian closure for the prediction of inertial-particle laden flows," *Communications in Computational Physics*, vol. 17, no. 1, pp. 1-46, 2015.
- [22] C. Chalons, D. Kah, and M. Massot, "Beyond pressureless gas dynamics : Quadrature-based velocity moment models," *Communications in Mathematical Sciences*, vol. 10, no. 4, pp. 1241-1272, 2012.
- [23] N. Lupoglazoff and F. Vuillot, "Simulation numérique bidimensionnelle des écoulements instationnaires dans les propulseurs à propergol solide," *La Recherche Aéronautique*, no. 2, pp. 21-41, 1992.
- [24] E. Daniel, "Eulerian approach for unsteady two-phase solid rocket flows with aluminum particles," *J. of Propulsion and Power*, vol. 16, no. 2, pp. 309-317, 2000.
- [25] M. Simoes, *Modélisation eulérienne de la phase dispersée dans les moteurs à propergol solide, avec prise en compte de la pression particulaire*. PhD thesis, Institut National Polytechnique de Toulouse, 2006.

- [26] V. Morfouace and P.-Y. Tissier, “Two-phase flow analysis of instabilities driven by vortex-shedding in solid rocket motors,” in 31st *AIAA/ASME/SAE/ASEE Joint Propulsion Conference and Exhibit*, AIAA Paper 95-2733, pp. 1–11, July 1995. San Diego, CA.
- [27] J. Dupays, *Contribution à l’étude du rôle de la phase condensée dans la stabilité d’un propulseur à propergol solide pour lanceur spatial*. PhD thesis, Institut National Polytechnique de Toulouse, 1996.
- [28] A. Kourta, “Computation of vortex shedding in solid rocket motors using time-dependant turbulence model,” *Journal of Propulsion and Power*, vol. 15, no. 3, pp. 390–400, 1999.
- [29] E. Daniel, R. Saurel, M. Larini, and J. Loraud, “A comparison between centered and upwind schemes for two-phase compressible flows,” in 29th *AIAA/SAE/ASME/ASEE Joint Propulsion Conference and Exhibit*, AIAA Paper 93–2346, June 1993. Monterey, CA.
- [30] C. Le Touze, A. Murrone, and H. Guillard, “Multislope MUSCL method for general unstructured meshes,” *Journal of Computational Physics*, vol. 284, pp. 389–418, 2015.
- [31] F. Vuillot and N. Lupoglazoff, “Combustion and turbulent flow effects in 2D unsteady Navier-Stokes simulations of oscillatory solid rocket motors - First applications,” in 34th *AIAA Aerospace Sciences Meeting and Exhibit*, AIAA Paper 96–0884, pp. 1–15, January 1996. Reno, NV.
- [32] S. de Chaisemartin, L. Fréret, D. Kah, F. Laurent, R. Fox, J. Reveillon, and M. Massot, “Eulerian models for turbulent spray combustion with polydispersity and droplet crossing,” *Comptes Rendus Mécanique*, vol. 337, pp. 438–448, 2009. Special Issue ‘Combustion for Aerospace Propulsion’.
- [33] F. Bouchut, S. Jin, and X. Li, “Numerical approximations of pressureless and isothermal gas dynamics,” *SIAM J. Num. Anal.*, vol. 41, pp. 135–158, 2003.
- [34] M. Duarte, M. Massot, S. Descombes, C. Tenaud, T. Dumont, V. Louvet, and F. Laurent, “New resolution strategy for multi-scale reaction wave using time operator splitting, space adaptative multiresolution and dedicated high order implicit/explicit time integrators,” *SIAM J. Sci. Comp.*, vol. 34, no. 1, pp. A76–A104, 2011.
- [35] S. Gottlieb, “On high order strong stability preserving Runge–Kutta and multi step time discretizations,” *Journal of Scientific Computing*, vol. 25, no. 1, pp. 105–128, 2005.
- [36] R. MacCormack, “The effect of viscosity in hypervelocity impact cratering,” *Journal of spacecraft and rockets*, vol. 40, no. 5, pp. 757–763, 2003. reprinted from AIAA Paper 69–354, 1969.
- [37] A. Jameson and T. J. Baker, “Numerical solution of the Euler equations for complex configurations,” in 6th *AIAA Computational Fluid Dynamics Conference*, AIAA Paper 83–1929, July 1983. Danvers, MA.
- [38] E. F. Toro, *Riemann Solvers and Numerical Methods for Fluid Dynamics: A Practical Introduction*. Berlin, Heidelberg: Springer-Verlag Berlin Heidelberg, 2009.
- [39] B. van Leer, “Towards the ultimate conservative difference scheme. ii. monotonicity and conservation combined in a second-order scheme,” *Journal of Computational Physics*, vol. 14, no. 4, pp. 361–370, 1974.
- [40] T. Buffard and S. Clain, “Monoslope and multislope muscl methods for unstructured meshes,” *Journal of Computational Physics*, vol. 229, no. 10, pp. 3745–3776, 2010.
- [41] N. Lupoglazoff and F. Vuillot, “Numerical simulation of vortex-shedding phenomena in 2D test case solid rocket motors,” in 30th *AIAA Aerospace Sciences Meeting and Exhibit*, AIAA Paper 92–0776, pp. 1–10, January 1992. Reno, NV.
- [42] S. Temkin and R. Dobbins, “Attenuation and dispersion of sound by particulate-relaxation processes,” *The Journal of the Acoustical Society of America*, vol. 40, no. 2, pp. 317–324, 1966.
- [43] S. Vincent, J.-P. Caltagirone, and P. Bonneton, “Numerical modelling of bore propagation and run-up on sloping beaches using a MacCormack TVD scheme,” *Journal of hydraulic research*, vol. 39, no. 1, pp. 41–49, 2001.